Distributed secondary control for proportional power sharing and DC bus voltage restoration in standalone DC microgrid

Phan-Thanh Nguyen[1], Duc Minh Pham[2]
[1]Department of Industrial Electricity, Faculty of Electrical and Electronics Engineering, Ho Chi Minh City University of Technology and Education, Ho Chi Minh City, Vietnam
[2]Power Electronics Research Laboratory, Faculty of Electrical and Electronics Engineering, Ho Chi Minh City University of Technology (HCMUT), VNU-HCM, Ho Chi Minh City, Vietnam

ABSTRACT

This article proposes a distributed secondary control scheme based on the voltage-shifting method for standalone direct current (DC) microgrids to enforce proportional power-sharing under the imbalance of the feeder line impedances and compensate for the DC bus voltage error caused by the droop control. Secondary control will be implemented on local controllers to increase reliability. A low-bandwidth communication network will also be needed to exchange converters' information. Using information from the communication network, the reference voltage for the primary control will be adjusted to compensate for the droop control and line impedance influences. The appropriate voltage shifting terms will be determined by the delta iteration method. The proposed control will be evaluated with simulations using PLECS software.

This is an open access article under the CC BY-SA license.

Corresponding Author:

Duc Minh Pham
Power Electronics Research Laboratory, Faculty of Electrical and Electronics Engineering
Ho Chi Minh City University of Technology (HCMUT), VNU-HCM
Ho Chi Minh City, Vietnam
Email: pmduc@hcmut.edu.vn

1. INTRODUCTION

The demand for electrical power has and will continue to increase as humanity grows in population and technological advancement. Thus, the requirement for power systems' reliability also increases [1]-[3]. Besides, the depletion of fossil fuel sources and their environmental concerns are forcing the energy industry to take a shift toward more sustainable renewable energy sources (RES). However, integrating Renewable Energy Sources into the utility grid is not as straightforward as it would seem. Due to the nature of RES, control and planning for the power system are difficult [1], [3]. In power generation methods involving synchronous generators, their transient characteristic and stability are dictated by the inertia constant [4]. However, RES are interfaced using power electronic devices, so RES either: i) are inertia-free and ii) have their inertia heavily influenced by the chosen control strategy. Either way, this causes the equivalent inertia of the system to be convoluted and difficult to evaluate, so RES integration needs proper planning [3], [4]. While RES has certain restrictions on location, they can be located near the consumer due to their low pollution regarding noise, exhaust, and safety concerns, making RES suitable for distributed generation (DG) plans to increase reliability and reduce transmission losses [5]-[7]. The increase in requirement for power systems, and the increase in RES' penetration has introduced the concept of microgrids.

The premise of a microgrid is a self-contained power distribution system with a defined boundary, consisting of local power generation sources, energy storage systems (ESS), and local loads [1]-[3].

A microgrid can be varied in scale, ranging from a single building to a residential area [8], [9]. Figure 1 illustrates the configuration of a direct current (DC) microgrid, showcasing the interconnectedness of local power generation sources, energy storage systems, and loads sharing a common DC bus. By having its own generators and storage, a microgrid is capable of operating both with and without connecting to the utility grid, thus increasing flexibility and reliability. Moreover, this also solves the problem of high-RES integration [3]. Based on their form of power transmission, microgrids are classified into alternating current (AC), DC, and hybrid microgrids.
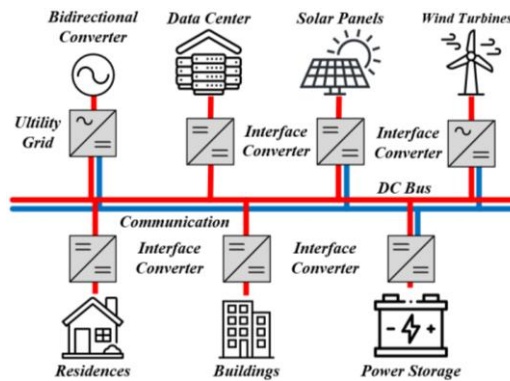

Figure 1. Structure of a DC microgrid

DC microgrids, which were made possible by the advancement in the field of power electronics in recent decades [1], [3], have some key advantages [9]. Transmitting DC power means less power losses and simpler control [10]-[13]. DC microgrids also theoretically reduce the converter stages needed since a large portion of electrical devices need AC-DC adapters to operate [3]. Also, power storage systems need DC input [14], [15] and popular RES exhibit DC output. A simple structure for a DC microgrid and its key components is shown in First is the bidirectional converter (BiC) for connecting the microgrid to the utility grid. Second is the main bus for linking the microgrid's converters. Depending on the scale and the requirement, more buses may be employed. Third are converters for interfacing the DC bus with generators, storage, and loads. Finally, a communication network for monitoring and controlling the microgrid.

A multi-layer hierarchical control structure is usually employed for controlling the microgrid [1], [16]-[20]. The primary control layer is for controlling the converters. At this layer, the droop control method is usually implemented due to its decent performance and simplicity. However, its performance will suffer greatly if line impedances are imbalanced [20]-[23]. The secondary control layer is for compensating errors caused by the primary layer and achieving other control objectives [13], [24]. In this case, those objectives are DC bus restoration and proportional power sharing. The secondary control can either adjust the primary control's reference value or the droop control coefficient to achieve these goals. There are restrictions on modifying the droop control coefficients since they heavily influence the system's transient response. As for the reference value modifying method, or the voltage shifting method in this case, such restriction is virtually non-existent because the reference value has minimal impact on the model of the system [23]-[26]. Therefore, voltage-shifting is a safe approach to the standalone DC microgrid problems. The implementation of the secondary control can be either distributed or centralized but the distributed implementation is often more favorable. Centralized control, as its name implies, needs a central controller. This central controller will compute voltage-shifting terms and then send them back to the corresponding primary controller. Having the whole system rely on a single central controller reduces its reliability because if that controller fails, the entire system will fail.

To avoid this shortcoming, multiple controllers are used. For the distributed control, the secondary controller will be implemented on each converter. Each converter is controlled by a distributed controller, consisting of the primary controller and its corresponding secondary controller, which will control the converter and compute its voltage-shifting term, increasing the system's reliability. This article proposed a distributed secondary control based on the voltage-shifting method for standalone DC microgrids to restore the DC bus voltage and maintain the proportional power-sharing under feeder lines impedance imbalance. This article is outlined as follows. Section 2 presents the problems mentioned. Section 3 presents the proposed control. Section 4 conducts a small-signal analysis for the proposed control. Section 5 presents the simulation results. Section 6 will conclude this article.

2. ANALYSIS OF THE DROOP CONTROL METHOD IN STANDALONE DC MICROGRID

Figure 2(a) presents the simplified model of a standalone DC microgrid with two generation units. Converters are represented as ideal voltage sources. The droop control method is applied by adjusting the converters' reference voltage according to their output current values. The characteristic lines of the applied droop control are represented in Figure 2(b). In Figures 2(a) and (b), V_o^* is the DC bus reference voltage and $R_{\mu G}$ is the load, while $V_{o1}^*, V_{o2}^*, v_{o1}, v_{o2}, i_{o1}, i_{o2}, r_1, r_2, R_{d1}, R_{d2}$ are the converters' nominal voltage, output voltage, output current, line impedance, and droop control coefficient of the converters, respectively. The expression for the output voltage and output current of the converters is obtained as (1)-(3):

$$v_{o1} = V_{o1}^* = V_o^* - i_{o1}R_{d1}$$
$$v_{o2} = V_{o2}^* = V_o^* - i_{o2}R_{d2} \tag{1}$$

$$i_{o1} = \frac{V_o^*(R_{d2}+r_2)}{R_{eq}} \tag{2}$$
$$i_{o2} = \frac{V_o^*(R_{d1}+r_1)}{R_{eq}}$$

$$R_{eq} = R_{\mu G}(R_{d1} + r_1 + R_{d2} + r_2) + (R_{d1} + r_1)(R_{d2} + r_2) \tag{3}$$

The output powers are expressed as (4):

$$P_{o1} = \frac{V_o^{*2}(R_{d2}+r_2)}{R_{eq}} - R_{d1}\left[\frac{V_o^*(R_{d2}+r_2)}{R_{eq}}\right]^2 \tag{4}$$
$$P_{o2} = \frac{V_o^{*2}(R_{d1}+r_1)}{R_{eq}} - R_{d2}\left[\frac{V_o^*(R_{d1}+r_1)}{R_{eq}}\right]^2$$

The ratio of the output powers is (5):

$$\frac{P_{o1}}{P_{o2}} = \frac{R_{eq}(R_{d2}+r_2)-R_{d1}(R_{d2}+r_2)^2}{R_{eq}(R_{d1}+r_1)-R_{d2}(R_{d1}+r_1)^2} \tag{5}$$

If the line impedances are insignificant to the droop control coefficients, (5) can be approximated to as (6):

$$\frac{P_{o1}}{P_{o2}} \approx \frac{R_{eq}R_{d2}-R_{d1}R_{d2}^2}{R_{eq}R_{d1}-R_{d2}R_{d1}^2} = \frac{R_{d2}(R_{eq}-R_{d1}R_{d2})}{R_{d1}(R_{eq}-R_{d1}R_{d2})} = \frac{R_{d2}}{R_{d1}} \tag{6}$$

In certain situations, the traditional droop control method can offer good power-sharing performance. However, this performance is not holding up very well as line impedances are often unknown so the droop control coefficients are difficult to choose correctly to negate the line impedances. Another point to make is the droop control coefficients' value has limits, as those coefficients could hamper the system's response, and since there is no voltage shifting, the DC bus voltage is guaranteed to be lower than its reference value. To compensate for the voltage, drop on the DC bus, a shifting term can be added to the primary control's reference. With voltage shifting terms applied, the converters' output voltage is (7):

$$v_{o1} = V_o^* + \delta V_1 - i_{o1}R_{d1}$$
$$v_{o2} = V_o^* + \delta V_2 - i_{o2}R_{d2} \tag{7}$$

In which $\delta V_1, \delta V_2$ are the voltage-shifting terms applied to the respective converters. The converters' output powers are (8):

$$P_{o1} = \frac{(V_o^*+\delta V_1)^2(R_{d2}+r_2)+R_{\mu G}(V_o^*+\delta V_1)(\delta V_1-\delta V_2)}{R_{eq}} - R_{d1}\left[\frac{(V_o^*+\delta V_1)(R_{d2}+r_2)+R_{\mu G}(\delta V_1-\delta V_2)}{R_{eq}}\right]^2 \tag{8}$$
$$P_{o2} = \frac{(V_o^*+\delta V_2)^2(R_{d1}+r_1)+R_{\mu G}(V_o^*+\delta V_2)(\delta V_2-\delta V_1)}{R_{eq}} - R_{d2}\left[\frac{(V_o^*+\delta V_2)(R_{d1}+r_1)+R_{\mu G}(\delta V_2-\delta V_1)}{R_{eq}}\right]^2$$

The output power ratio is rewritten as (9):

$$\frac{P_{o1}}{P_{o2}} = \frac{a_0\delta V_1^2+a_1\delta V_1+a_2\delta V_1\delta V_2+a_3\delta V_2+a_4\delta V_2^2+a_5}{b_0\delta V_1^2+b_1\delta V_1+b_2\delta V_1\delta V_2+b_3\delta V_2+b_4\delta V_2^2+b_5} \tag{9}$$

In which:

$$a_0 = \left[R_{eq} - R_{d1}(R_{d2} + r_2)\right](R_{d2} + r_2) + R_{\mu G}R_{eq} - R_{d1}R_{\mu G}{}^2$$
$$a_1 = 2V_o^*\left[R_{eq} - R_{d1}(R_{d2} + r_2)\right](R_{d2} + r_2) + R_{\mu G}R_{eq}V_o^*$$
$$a_2 = -R_{\mu G}R_{eq} + 2R_{d1}R_{\mu G}{}^2; a_3 = -R_{\mu G}R_{eq}V_o^*; a_4 = -R_{d1}R_{\mu G}{}^2; a_5 = \left[R_{eq} - R_{d1}(R_{d2} + r_2)\right](R_{d2} + r_2)V_o^{*2}$$
$$b_0 = -R_{d2}R_{\mu G}{}^2; b_1 = -R_{\mu G}R_{eq}V_o^*; b_2 = -R_{\mu G}R_{eq} + 2R_{d2}R_{\mu G}{}^2$$
$$b_3 = 2V_o^*\left[R_{eq} - R_{d2}(R_{d1} + r_1)\right](R_{d1} + r_1) + R_{\mu G}R_{eq}V_o^*$$
$$b_4 = \left[R_{eq} - R_{d2}(R_{d1} + r_1)\right](R_{d1} + r_1) + R_{\mu G}R_{eq} - R_{d2}R_{\mu G}{}^2; b_5 = \left[R_{eq} - R_{d2}(R_{d1} + r_1)\right](R_{d1} + r_1)V_o^{*2}$$

From the expression obtained in (9), it can be inferred that the output power ratio can be controlled by applying appropriate voltage shifting terms.
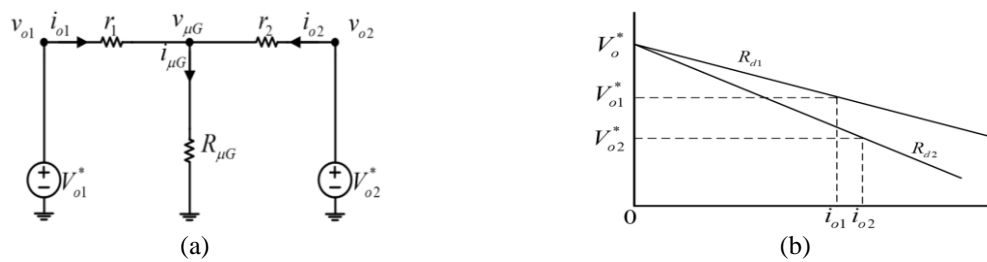

Figure 2. DC microgrid simplified model and the droop characteristic; (a) simplified model and (b) output current–reference voltage droop characteristic

3. PROPOSED CONTROL ALGORITHM

3.1. Proposed secondary control

Figures 3(a) and (b) present the proposed control diagram and proposed flowchart, respectively. The proposed distributed control's objective is to ensure proportional power sharing under line impedance imbalance and compensate for the voltage drop on the DC bus caused by the droop control method. To achieve these goals, distributed controllers need to i) receive DC bus voltage readings and ii) exchange information with neighboring converters. The exchanging information is defined as (10):

$$P.U_i = \frac{P_{oi}}{P_{Ri}} \tag{10}$$

In which $P.U_i$ is the output power per unit and P_{Ri} is the maximum output power of the *i*th converter. The secondary control runs at a lower rate compared to the primary control due to communication. At the start of each secondary control cycle, the distributed controller broadcasts its information on the communication network and receives other converters' information. Based on the information received, the number of neighboring converters is determined. While it can be predetermined, due to the delay and the possibility of communication failure, the number of neighbors should be dynamically determined for each control cycle. After determining the number of neighbors *N*, the distributed controller will calculate the average output power per unit $\overline{P.U}$ of its cluster as (11):

$$\overline{PU} = \sum_{i=1}^{N} \frac{P.U_i}{N} \tag{11}$$

The voltage shifting term is then determined through the delta iteration method as (12)-(14):

$$\delta V_i = \delta V_{\Delta Pi} + \delta V_{\Delta Vi} \tag{12}$$

$$\delta V_{\Delta Pi}(k) = \delta V_{\Delta Pi}(k-1) + T\left[V_o^* - V_o^* \frac{PU_i(k)}{\overline{P.U}(k)}\right] \tag{13}$$

$$\delta V_{\Delta Vi}(k) = \delta V_{\Delta Vi}(k-1) + T\left[V_o^* - V_{\mu G}(k)\right] \tag{14}$$
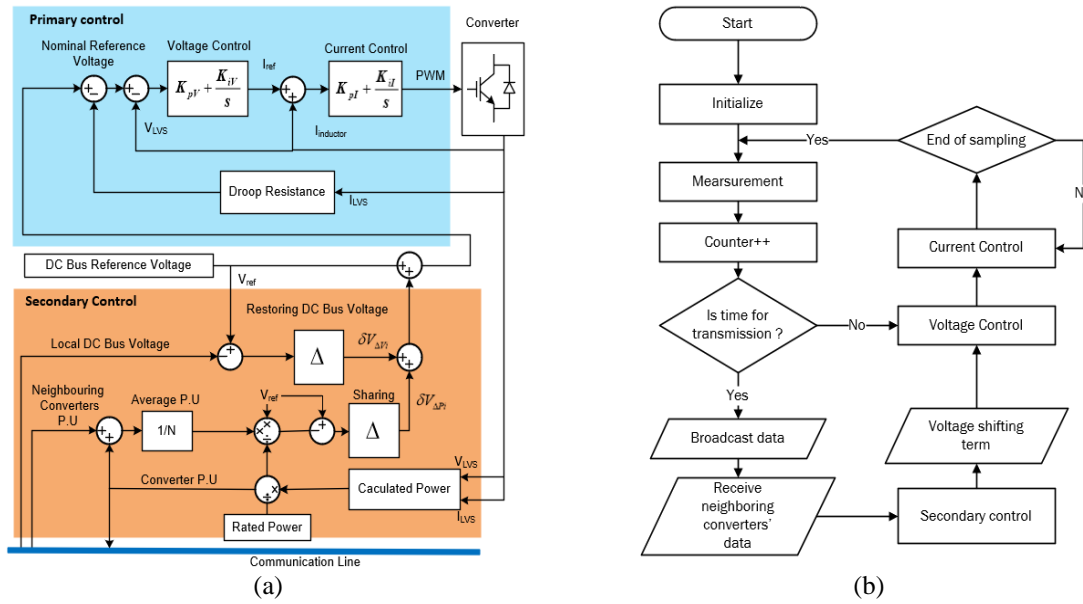
Figure 3. Proposed control diagram and flowchart; (a) diagram and (b) flowchart

3.2. Design of the primary control

In this article, the buck converters are used. For the primary control, the cascaded proportional integral (PI) control structure with droop control is implemented for better transient [27], [28]. This control structure employs two PI compensators in series. The outer controller is the voltage controller and the inner controller is the current controller. The voltage controller is described as (15):

$$I_{Liref} = \left(K_{PVi} + \frac{K_{IVi}}{s}\right)(V_{oi}^* - v_{oi}) \tag{15}$$

In which I_{Liref} is the reference for the inductor current of the ith converter and K_{PVi}, K_{IVi} are voltage controller parameters of the ith converter. The current controller is described as (16):

$$d_i = \left(K_{PCi} + \frac{K_{ICi}}{s}\right)(I_{Liref} - I_{Li}) \tag{16}$$

In which d_i is the duty cycle for the ith converter and K_{PCi}, K_{ICi}, I_{Li} are the current controller parameters and inductor current of the ith converter. Voltage controller and current controller parameters are chosen based on the analysis conducted in [27]. The voltage controller's parameters are chosen as (17):

$$K_{PV} = \frac{1}{R}$$
$$K_{IV} = \frac{1}{R^2C} \tag{17}$$

In which R is the load and C is the output capacitor. The current controller is designed as (18) and (19):

$$\omega_n = \frac{1}{RC} \tag{18}$$

$$K_{PI} = \frac{2N\omega_n L}{V_i}$$
$$K_{II} = \frac{N^2 \omega_n^2 L}{V_i} \tag{19}$$

In which ω_n is the voltage loop undamped natural frequency, V_i is the voltage supply to the converter, L is the converter's inductor. For the cascade control, the inner loop has to be N times dynamically faster than the outer loop. In the case of the Buck converter, the current loop needs to be at least four times faster than the voltage loop [27]. In DC microgrids, the load varies so to prevent overdamping the voltage loop, the highest output current will be considered when calculating parameters. The highest output current

expected for each converter also varies based on their rated output power. Thus, each converter may have a different set of controller parameters while being physically identical.

4. SMALL-SIGNAL ANALYSIS

The output voltages in Figure 2 can also be expressed as (20):

$$\begin{bmatrix} v_{o1} \\ v_{o2} \end{bmatrix} = \begin{bmatrix} r_1 + R_{\mu G} & R_{\mu G} \\ R_{\mu G} & r_2 + R_{\mu G} \end{bmatrix} \begin{bmatrix} i_{o1} \\ i_{o2} \end{bmatrix} \tag{20}$$

The output current is (21):

$$\begin{bmatrix} i_{o1} \\ i_{o2} \end{bmatrix} = \begin{bmatrix} \alpha_{11} & \alpha_{12} \\ \alpha_{21} & \alpha_{22} \end{bmatrix} \begin{bmatrix} v_{o1} \\ v_{o2} \end{bmatrix} = \begin{bmatrix} \frac{R_{\mu G}+r_2}{r_2 r_1 + r_1 R_{\mu G} + r_2 R_{\mu G}} & \frac{-R_{\mu G}}{r_2 r_1 + r_1 R_{\mu G} + r_2 R_{\mu G}} \\ \frac{-R_{\mu G}}{r_2 r_1 + r_1 R_{\mu G} + r_2 R_{\mu G}} & \frac{R_{\mu G}+r_1}{r_2 r_1 + r_1 R_{\mu G} + r_2 R_{\mu G}} \end{bmatrix} \begin{bmatrix} v_{o1} \\ v_{o2} \end{bmatrix} \tag{21}$$

The delta iteration in (13) and (14) can be rewritten in the form of the output u and the error e as (22):

$$u(k) = u(k-1) + Te(k) \tag{22}$$

Or:

$$G_{itr}(s) = \frac{\frac{T}{2}s+1}{s} \tag{23}$$

With G_{itr} being the continuous representation of the delta iteration implemented as the secondary control, T is sampling time. Figure 4 presents the control diagram for converter 1 in a system of two converters. Since the current loop's dynamic is significantly faster than the voltage loop, the current loop is represented as a first-order process to simplify the small-signal analysis [25], [29]. Assuming the primary control takes much less time to settle compared to the secondary control interval, the converters are now equal to voltage sources from the secondary control perspective. Converter 1 closed-loop transfer function can be represented as (24):

$$G_{Vo1} = \frac{G_{PI}G_C}{1+G_{PI}G_C} \tag{24}$$

With G_{Vo1} being the converter close-loop transfer function, G_{PI} is the voltage loop's compensator and G_C is the current closed-loop transfer function. From Figure 2, the DC bus voltage can be expressed as (25):

$$\begin{aligned} V_{\mu G} &= v_{o1} - i_{o1}r_1 \\ &= v_{o1} - \alpha_{11}v_{o1}r_1 + \alpha_{12}v_{o2}r_1 \end{aligned} \tag{25}$$

According to Figure 4, the voltage-shifting term for converter 1 can be expressed as (26):

$$\delta V_1 = \left(V_o^* - e^{-t_d s}V_{\mu G}\right)G_{itr} + \left(V_o^* - V_o^* \frac{P.U_1}{P.U} e^{-t_d s}\right)G_{itr} \tag{26}$$

Substituting (25) into (26) yields as (27):

$$\delta V_1 = G_{itr}\left(2V_o^* - \frac{2V_o^* P.U_1}{P.U_1 + P.U_2}e^{-t_d s}\right) - v_{o1}G_{itr}e^{-t_d s}(1 - \alpha_{11}r_1) - v_{o2}G_{itr}\alpha_{12}r_1 e^{-t_d s} \tag{27}$$

The nominal reference voltage for converter 1 is (28):

$$\begin{aligned} V_{o1}^*(z) &= V_o^* + \delta V_1 - i_{o1}G_{LPF}R_{d1} \\ &= \left[V_o^* + G_{itr}V_o^*\left(2 - \frac{2P.U_1 e^{-t_d s}}{P.U_1 + P.U_2}\right)\right] - v_{o1}[G_{itr}e^{-t_d s}(1 - \alpha_{11}r_1) + \alpha_{11}G_{LPF}R_{d1}] + v_{o2}\alpha_{12}(G_{LPF}R_{d1} - G_{itr}r_1 e^{-t_d s}) \end{aligned} \tag{28}$$

With $G_{LPF}(s) = \frac{2\pi f_c}{s+2\pi f_c}$. From Figure 4, the output voltage of converter 1 as (29):

$$v_{o1}(z) = \frac{\left[V_o^*+G_{itr}V_o^*\left(2-\frac{2P.U_1 e^{-t_d s}}{P.U_1+P.U_2}\right)+v_{o2}\left(\alpha_{12}G_{LPF}R_{d1}-G_{itr}\alpha_{12}r_1 e^{-t_d s}\right)\right]G_{Vo1}}{1+\left[G_{itr}e^{-t_d s}(1-\alpha_{11}r_1)+\alpha_{11}G_{LPF}R_{d1}\right]G_{Vo1}} \tag{29}$$

Linearizing (29) to obtain the small-signal transfer function from nominal voltage to output voltage of converter 1 as (30):

$$\left.\frac{\hat{v}_{o1}}{\hat{V}_o^*}\right|_{\hat{v}_{o2}=0} = \frac{\left[V_o^*+G_{itr}V_o^*(2-2e^{-t_d s})\right]G_{Vo1}}{1+\left[G_{itr}e^{-t_d s}(1-\alpha_{11}r_1)+\alpha_{11}G_{LPF}R_{d1}\right]G_{Vo1}} \tag{30}$$
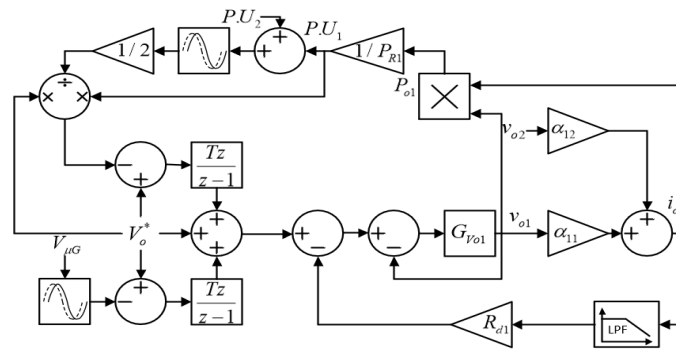
Figure 4. Control diagram for converter 1 in a system of two converters

Small-signal model is analyzed by varying important parameters such as load resistance, line impedance, droop coefficient, and communication delay of converter 1 to observe the poles' movement. The load $R_{\mu G}$ were varied from 5 Ω to 100 Ω. Line impedance r_1 were varied from 0.05 Ω to 3.0 Ω. The droop coefficient was varied from 0.5 Ω to 3.5 Ω. Communication delay t_d is varied from 1 ms to 1000 ms. coefficient R_{d1} were varied from 0.5 Ω to 3.5 Ω. When a parameter is being varied, others are kept at values described in Table 1.

Figures 5(a) and (b) display the pole maps of the results when increasing communication delay and droop coefficient, respectively. Similarly, Figures 5(c) and (d) llustrate the pole maps when increasing line impedance and load resistance, respectively. The poles of the small signal model are influenced by variations in parameters such as communication delay, droop coefficient, line impedance, and load resistance. However, within the range of values examined in this article, no small-signal instability is detected. Notably, the communication delay is more associated with complex poles than other parameters. When increasing the time delay, the poles' imaginary part also increases initially, but it seems that when passing a certain threshold, the imaginary part starts to decrease. While the communication time delay did affect the secondary control natural frequency, which dictates how much the system oscillates before it settles, it will not destabilize the system as the poles are still on the left-hand side of the s-plane.

Increasing the droop coefficient and line impedance have similar effects, as the poles tend to move toward the right-hand side of the s-plane, reducing the system damping, and thus increasing the settling time. As for load resistance, when increases, which means load power decreases, poles tend to move to the left, making the system settle faster. However, while the poles did move under the variation of load, it is just slightly noticeable, suggesting that changing the load has little impact on the system's dynamic. Figure 6 presents the control diagram for converter 1 in a system of N converters. Consider Figure 2 with N converters and expand (21):

$$[R][i_o] = [v_o] \Leftrightarrow \begin{bmatrix} R_{\mu G}+r_1 & R_{\mu G} & \cdots & R_{\mu G} \\ R_{\mu G} & R_{\mu G}+r_2 & \cdots & R_{\mu G} \\ \vdots & \vdots & \vdots & \vdots \\ R_{\mu G} & R_{\mu G} & \cdots & R_{\mu G}+r_N \end{bmatrix}\begin{bmatrix} i_{o1} \\ i_{o2} \\ \vdots \\ i_{oN} \end{bmatrix} = \begin{bmatrix} v_{o1} \\ v_{o2} \\ \vdots \\ v_{oN} \end{bmatrix} \tag{31}$$

Output currents now related to output voltage as (32):

$$[i_o] = [R]^{-1}[v_o] = [\alpha][v_o] \tag{32}$$

As inferred from Figure 6 and (31), changing the number of converters is changing how the output voltages relate to output currents. Thus, the change in converter number mostly affects the coefficient α_{11} in (30). Therefore, this change should have similar effects compared to when the load, line impedances, or droop coefficients are being varied.

Table 1. Small-signal analysis parameter

Item	Symbol	Value
Voltage reference	V_o^*	48 V
Line impedance	r_1, r_2	0.3, 0.8 Ω
Droop coefficient	R_{d1}	1.0 Ω
Load	R_G	10 Ω
LPF cut-off frequency	f_c	1000 Hz
Communication delay	t_d	1ms
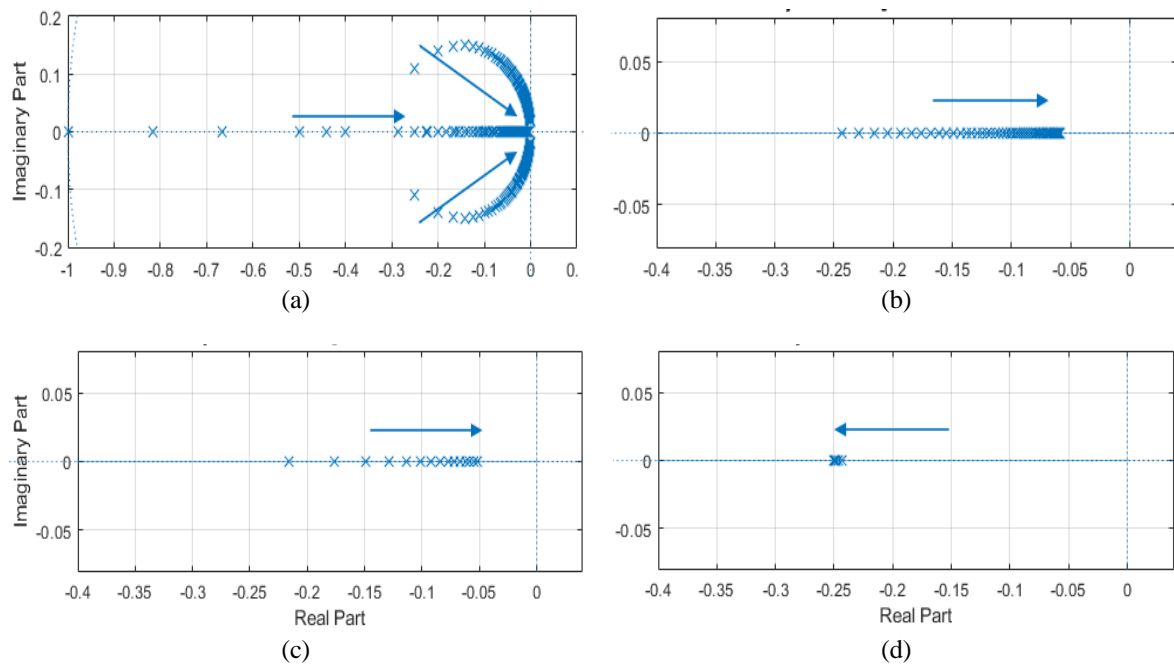
Figure 5. Close-loop system poles movement when increase; (a) communication delay, (b) droop coefficient, (c) line impedance, and (d) load resistance
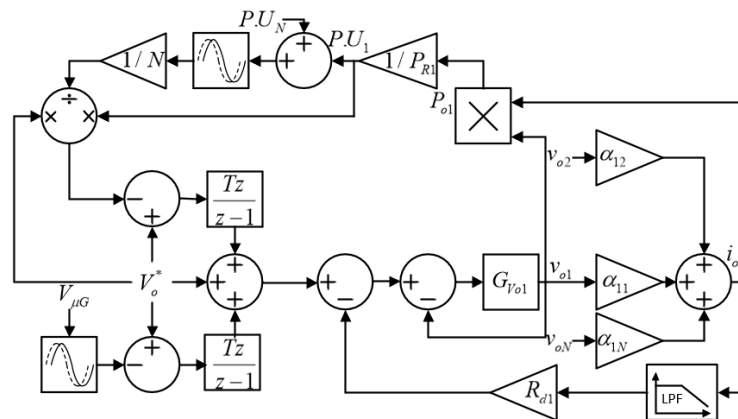
Figure 6. Control diagram for converter 1 in a generalized system with N converters

5. SIMULATION RESULTS

Table 2 presents the parameters which will be used in the simulated model described in Figure 7. The model consists of three converters with different rated power and three loads, two of which are detachable. The primary controllers are designed based on the expectation that each converter's output power is 300 W or below. The simulation starts with only load 1 and droop control. Simulation results are present from t=6 s to t=120 s.

Table 2. Simulation parameters

Item	Symbol	Value
Voltage reference	V_o^*	48 V
Rated power	P_{R1}, P_{R2}, P_{R3}	200 W, 250 W, 300 W
Line impedance	r_1, r_2, r_3	0.2, 0.4, 0.5 Ω
Droop resistance	R_{d1}, R_{d2}, R_{d3}	1.0, 1.0, 1.0 Ω
Load	R_1, R_2, R_3	15 Ω, 20 Ω, 25 Ω
Voltage PI compensator	PI controller	$k_p = 16.6, k_i = 0.125$
Current PI compensator	PI controller	$k_p = 11.7, k_i = 7780$
Switching frequency	f_{sw}	20 kHz
Secondary sampling	T	1 ms
Communication period	t_d	1 ms

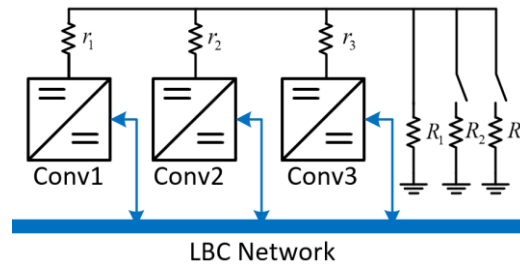Figure 7. Simulated model

Figure 8 presents the simulation result from t=6 s to t=56 s, which showcases the limit of traditional droop control and the initialization of the proposed secondary control as well as the proposed control response to load changes. From t=6 s to t=10 s, secondary control is disabled and the line impedances are severely imbalanced. Thus, the traditional droop control is unable to maintain the output-power ratio. At t=20 s, the droop coefficients are increased to (7.6:6.0:5.0) to mitigate the effect of line impedances. This set of droop coefficients is chosen based on (6) and converters' rated output in Table 2. While the output power is proportionally shared (0.217, 0.213, and 0.206 p.u), the DC bus voltage drop is further worsened. At t=20 s the droop control coefficients are reverted to the default value. At t=30 s, the secondary control is enabled and starts to compute voltage shifting terms. The DC bus voltage returns to its nominal value after 3 s. Proportional power sharing is achieved after 0.5 s and settles at 0.31 p.u. At t=40 s, the second load is connected and the third load is connected at t=50 s. The DC bus experienced minor voltage drops when a new load was connected but was able to maintain at nominal value. Proportional power sharing is achieved after 0.6 s and 0.7 s at 0.496 p.u and 0.598 p.u.

Figure 9 presents the simulation result from t=56 s to t=120 s, which simulate the communication failure and line failure on converter 2. At t=60 s, the second converter has a communication failure. This means only the first and the third converter will have their voltage shifting terms updated while the second converter will continue to operate with its previously calculated voltage shifting term. Although the communication failure occurred, due to the system already settled when the failure happened, no observable change was detected. At t=70 s, the third load is disconnected. The voltage shifting terms of the first and the third converter are updated and their output power per unit converged after 0.25 s and settled at 0.423 p.u while the second converter's output remains unchanged. At t=80 s, the second converter's communication is restored. The DC bus voltage has no significant change and the output power per unit converged after 0.7 s and then settled at 0.469 p.u. At t=90 s, line failure occurred at the second converter. The DC bus suffered a voltage drop but recovered after 2.8 s. Much similar to the communication failure, only the first and the third converter are considered for secondary control. Output power is proportionally shared after 0.3 s and settled at 0.646 p.u. At t=100 s, the second load is detached. The DC bus voltage has a voltage spike but can recover

after 4.6 s. Proportional power sharing is attained after 0.2 s at 0.426 p.u. It can be seen that changing the number of converters did affect the system's response as the DC bus voltage took much longer to settle. At t=110 s, the second converter is connected. The DC bus recovered from the voltage drop after 4.6 s and proportional power sharing is achieved after 0.6 s at 0.31 p.u.
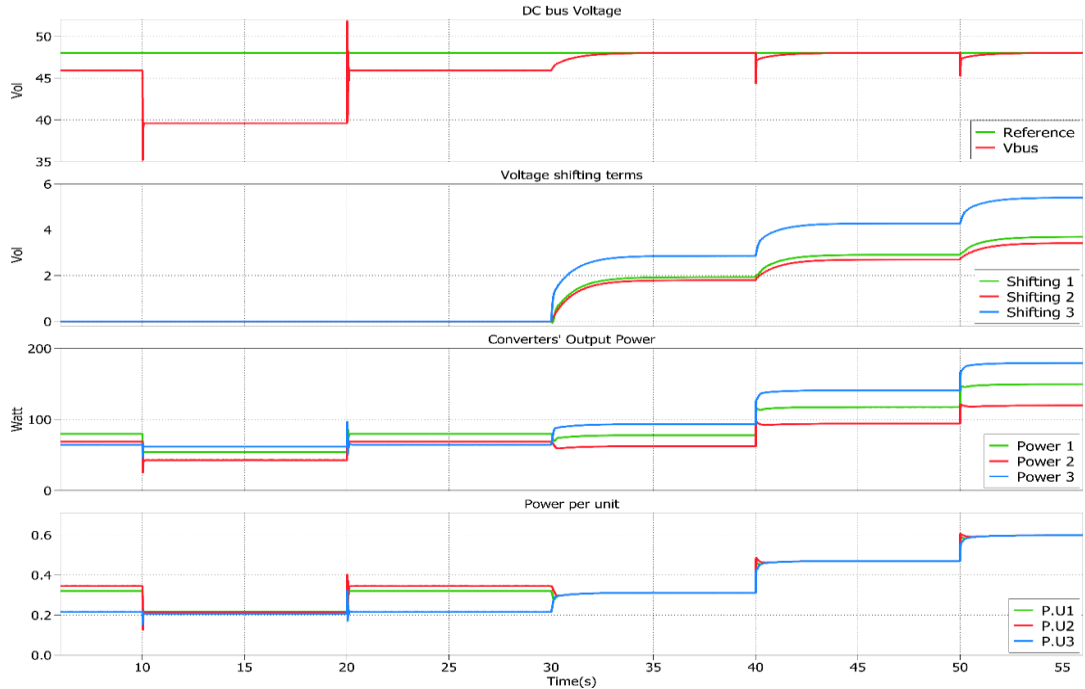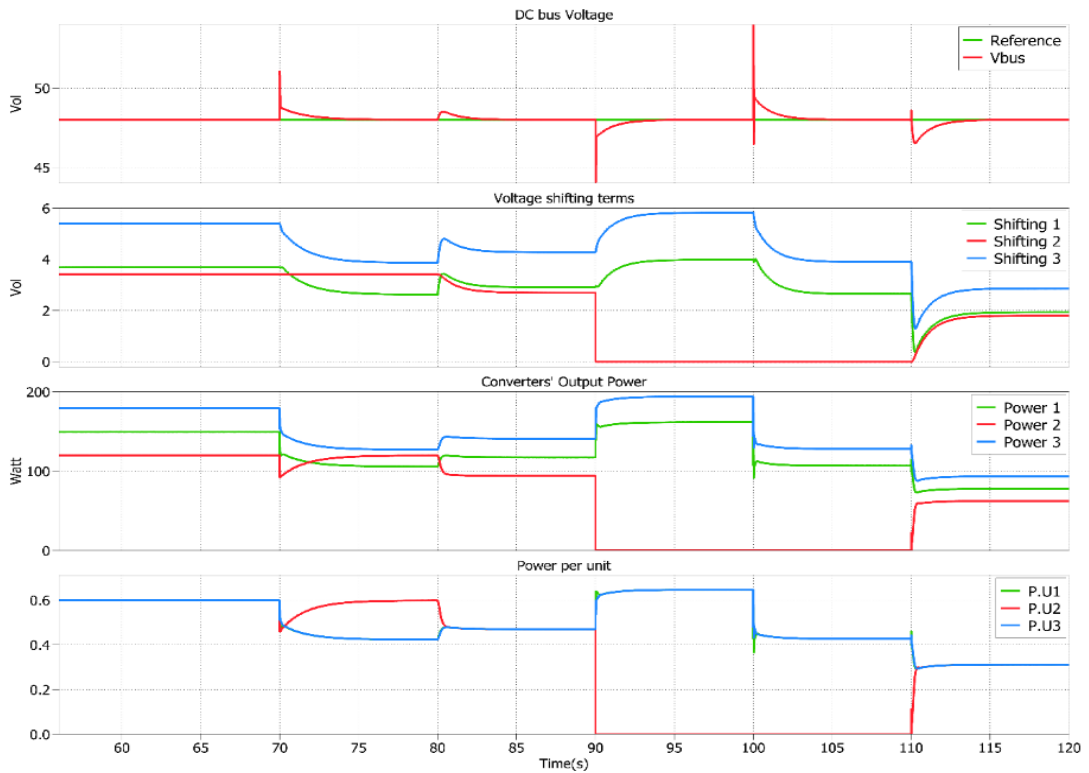

Figure 8. Simulation result from t=6 s to t=56 s

Figure 9. Simulation result from t=56 s to t=120 s

6. CONCLUSION

This article proposes a distributed secondary control scheme based on the voltage-shifting method for standalone DC microgrids to ensure proportional power-sharing under the imbalance of the feeder line impedances and compensate for the DC bus voltage deviation caused by the droop control. The secondary control is implemented using the delta iteration method to determine the appropriate voltage shifting terms based on the information received from the communication network. Small-signal analysis is conducted for the proposed control to evaluate its response to the variation of operating conditions. It is deducted from the small-signal analysis that while the system settling time is affected by the time delay, it will not be destabilized regardless of the time delay. The proposed control is evaluated using a PLECS simulation model. The proposed control proved its effectiveness over the traditional droop control under the line impedance imbalance. The proposed control is also tested in possible operating conditions such as load changes, communication failure, and converter connects/disconnects.

REFERENCES

[1] F. S. Al-Ismail, "DC Microgrid Planning, Operation, and Control: A Comprehensive Review," *IEEE Access*, vol. 9, pp. 36154–36172, 2021, doi: 10.1109/ACCESS.2021.3062840.
[2] A. T. Elsayed, A. A. Mohamed, and O. A. Mohammed, "DC microgrids and distribution systems: An overview," *Electric Power Systems Research*, vol. 119, pp. 407–417, Feb. 2015, doi: 10.1016/j.epsr.2014.10.017.
[3] T. Ma, H. Yahoui, H. Vu, N. Siauve, and H. Morel, "A Control Strategy of DC Building Microgrid Connected to the Neighborhood and AC Power Network," *Buildings*, vol. 7, no. 4, p. 42, May 2017, doi: 10.3390/buildings7020042.
[4] J. Zhang and H. Xu, "Online Identification of Power System Equivalent Inertia Constant," *IEEE Transactions on Industrial Electronics*, vol. 64, no. 10, pp. 8098–8107, Oct. 2017, doi: 10.1109/TIE.2017.2698414.
[5] B. Singh and J. Sharma, "A review on distributed generation planning," *Renewable and Sustainable Energy Reviews*, vol. 76, pp. 529–544, Sep. 2017, doi: 10.1016/j.rser.2017.03.034.
[6] S. N Singh, "Distributed Generation in Power Systems: An Overview and Key Issues," 2009.
[7] A. Yadav and L. Srivastava, "Optimal placement of distributed generation: An overview and key issues," in *2014 International Conference on Power Signals Control and Computations (EPSCICON)*, Jan. 2014, pp. 1–6, doi: 10.1109/EPSCICON.2014.6887517.
[8] S. Ali, Z. Zheng, M. Aillerie, J. P. Sawicki, M. C. Péra, and D. Hissel, "A review of dc microgrid energy management systems dedicated to residential applications," *Energies*, vol. 14, no. 14, 2021, doi: 10.3390/en14144308.
[9] H. Kakigano, Y. Miura, T. Ise, T. Momose, and H. Hayakawa, "Fundamental characteristics of DC microgrid for residential houses with cogeneration system in each house," in *IEEE Power and Energy Society 2008 General Meeting: Conversion and Delivery of Electrical Energy in the 21st Century, PES*, Jul. 2008, pp. 1–8, doi: 10.1109/PES.2008.4596210.
[10] S. Beheshtaein, R. M. Cuzner, M. Forouzesh, M. Savaghebi, and J. M. Guerrero, "DC Microgrid Protection: A Comprehensive Review," *IEEE Journal of Emerging and Selected Topics in Power Electronics*, pp. 1–1, 2019, doi: 10.1109/JESTPE.2019.2904588.
[11] F. Mohan and N. Sasidharan, "Protection of low voltage DC microgrids: A review," *Electric Power Systems Research*, vol. 225, p. 109822, Dec. 2023, doi: 10.1016/j.epsr.2023.109822.
[12] A. Chandra, G. K. Singh, and V. Pant, "Protection techniques for DC microgrid- A review," *Electric Power Systems Research*, vol. 187, p. 106439, Oct. 2020, doi: 10.1016/j.epsr.2020.106439.
[13] A. El-Shahat and S. Sumaiya, "DC-Microgrid System Design, Control, and Analysis," *Electronics*, vol. 8, no. 2, p. 124, Jan. 2019, doi: 10.3390/electronics8020124.
[14] S. O. Amrouche, D. Rekioua, and T. Rekioua, "Overview of energy storage in renewable energy systems," in *2015 3rd International Renewable and Sustainable Energy Conference (IRSEC)*, Dec. 2015, pp. 1–6, doi: 10.1109/IRSEC.2015.7454988.
[15] H. Lund *et al.*, "Energy storage and smart energy systems," *International Journal of Sustainable Energy Planning and Management*, vol. 11, pp. 3–14, 2016, doi: 10.5278/ijsepm.2016.11.2.
[16] C. Jin, P. Wang, J. Xiao, Y. Tang, and F. H. Choo, "Implementation of Hierarchical Control in DC Microgrids," *IEEE Transactions on Industrial Electronics*, vol. 61, no. 8, pp. 4032–4042, Aug. 2014, doi: 10.1109/TIE.2013.2286563.
[17] J. M. Guerrero, J. C. Vasquez, J. Matas, L. G. de Vicuna, and M. Castilla, "Hierarchical Control of Droop-Controlled AC and DC Microgrids—A General Approach Toward Standardization," *IEEE Transactions on Industrial Electronics*, vol. 58, no. 1, pp. 158–172, Jan. 2011, doi: 10.1109/TIE.2010.2066534.
[18] Y. Han, X. Ning, P. Yang, and L. Xu, "Review of Power Sharing, Voltage Restoration and Stabilization Techniques in Hierarchical Controlled DC Microgrids," *IEEE Access*, vol. 7, pp. 149202–149223, 2019, doi: 10.1109/ACCESS.2019.2946706.
[19] C. N. Papadimitriou, E. I. Zountouridou, and N. D. Hatziargyriou, "Review of hierarchical control in DC microgrids," *Electric Power Systems Research*, vol. 122, pp. 159–167, May 2015, doi: 10.1016/j.epsr.2015.01.006.
[20] U. B. Tayab, M. A. Bin Roslan, L. J. Hwai, and M. Kashif, "A review of droop control techniques for microgrid," *Renewable and Sustainable Energy Reviews*, vol. 76, pp. 717–727, Sep. 2017, doi: 10.1016/j.rser.2017.03.028.
[21] F. Chen, R. Burgos, D. Boroyevich, and W. Zhang, "A nonlinear droop method to improve voltage regulation and load sharing in DC systems," in *2015 IEEE First International Conference on DC Microgrids (ICDCM)*, Jun. 2015, pp. 45–50, doi: 10.1109/ICDCM.2015.7152008.
[22] G. Xu, D. Sha, and X. Liao, "Decentralized Inverse-Droop Control for Input-Series–Output-Parallel DC–DC Converters," *IEEE Transactions on Power Electronics*, vol. 30, no. 9, pp. 4621–4625, Sep. 2015, doi: 10.1109/TPEL.2015.2396898.

[23] W. W. A. G. Silva, T. R. Oliveira, and P. F. Donoso-Garcia, "An Improved Voltage-Shifting Strategy to Attain Concomitant Accurate Power Sharing and Voltage Restoration in Droop-Controlled DC Microgrids," *IEEE Transactions on Power Electronics*, vol. 36, no. 2, pp. 2396–2406, Feb. 2021, doi: 10.1109/TPEL.2020.3009619.

[24] F. GAO, R. KANG, J. CAO, and T. YANG, "Primary and secondary control in DC microgrids: a review," *Journal of Modern Power Systems and Clean Energy*, vol. 7, no. 2, pp. 227–242, Mar. 2019, doi: 10.1007/s40565-018-0466-5.

[25] K. D. Hoang and H.-H. Lee, "Accurate Power Sharing with Balanced Battery State of Charge in Distributed DC Microgrid," *IEEE Transactions on Industrial Electronics*, vol. 66, no. 3, pp. 1883–1893, Mar. 2019, doi: 10.1109/TIE.2018.2838107.

[26] Duy-Hung Dam, Hong-Hee Lee, and Heung-Geun Kim, "Effective output voltage quality control under nonlinear loads in islanded microgrid," in *2015 IEEE 2nd International Future Energy Electronics Conference (IFEEC)*, Nov. 2015, pp. 1–6, doi: 10.1109/IFEEC.2015.7361497.

[27] K. M. Tsang and W. L. Chan, "Cascade controller for DC/DC buck convertor," *IEE Proceedings - Electric Power Applications*, vol. 152, no. 4, p. 827, 2005, doi: 10.1049/ip-epa:20045198.

[28] S. Ansari, J. Zhang, and K. Iqbal, "Modeling, Stability Analysis and Simulation of Buck Converter in a DC Microgrid," in *2021 IEEE Kansas Power and Energy Conference (KPEC)*, Apr. 2021, pp. 1–4, doi: 10.1109/KPEC51835.2021.9446255.

[29] X. Lu, J. M. Guerrero, K. Sun, and J. C. Vasquez, "An Improved Droop Control Method for DC Microgrids Based on Low Bandwidth Communication with DC Bus Voltage Restoration and Enhanced Current Sharing Accuracy," *IEEE Transactions on Power Electronics*, vol. 29, no. 4, pp. 1800–1812, Apr. 2014, doi: 10.1109/TPEL.2013.2266419.

BIOGRAPHIES OF AUTHORS

Phan-Thanh Nguyen is currently a lecturer in the Faculty of Electronics and Electrical Engineering, Ho Chi Minh City University of Technology and Education. He obtained his Ph.D. in Electrical Engineering at Southern Taiwan University of Science and Technology, Taiwan, in 2016. His current research interests are intelligent control systems, automatic motion control, and electric drives. He can be contacted at email: thanhnp@hcmute.edu.vn.

Duc Minh Pham is currently a lecturer in the Faculty of Electrical and Electronics Engineering, Ho Chi Minh City University of Technology. He obtained his Ph.D. in Electrical Engineering at University of Ulsan, South Korea, in 2022. His current research interests are hybrid microgrid control systems, harmonic compensation, and electric drives. He can be contacted at email: pmduc@hcmut.edu.vn.